Performance Analysis of Intelligent Reflecting Surface-Aided Vehicular Communications under Dynamic Blockage

Diana Kujang SEMAYA, Wei CHEN, Changzhen LI *

School of Information Engineering, Wuhan University of Technology, Wuhan 430070, China

dianakujang@whut.edu.cn, greatchen@whut.edu.cn, *changzhen.li@whut.edu.cn

Submitted December 6, 2025 / Accepted February 20, 2026 / Online first March 12, 2026

Abstract. *Intelligent reflecting surfaces (IRS) promise coverage enhancement for vehicular networks, but optimal deployment strategies remain unclear. This paper analyzes where and when an IRS provides the greatest value under dynamic line-of-sight (LOS) and non-line-of-sight (NLOS) blockage transitions. Using a blockage model motivated by published mmWave vehicular measurements (three spatial NLOS zones with 15 dB direct-path attenuation) and Monte Carlo simulations, we quantify regime-dependent IRS gains, CSI requirements, and scaling with blockage severity. The key findings are: (i) in NLOS the IRS yields about a 10.8-fold rate gain, compared with about a 1.2-fold gain in LOS (roughly a ninefold difference in gain); (ii) CSI requirements in NLOS can be relaxed by approximately 13–27% while preserving most of the IRS benefit; (iii) IRS-assisted NLOS performance remains stable across a wide range of scattering conditions (Rician K between 0.5 and 10); and (iv) for a 256-element IRS the gain increases superlinearly with blockage severity and exceeds a twofold improvement once the blockage level is around 20 dB. These results suggest deployment guidelines that prioritize IRS placement at severely blocked locations (e.g., urban canyons and intersections), where the IRS impact is most pronounced.*

Keywords

Intelligent reflecting surface (IRS), V2X communications, dynamic blockage, LOS/NLOS transitions, channel state information

1. Introduction

Vehicular communication is essential for intelligent transportation systems, supporting safety-critical applications such as collision avoidance, cooperative driving, and traffic management [1]. The evolution toward sixth-generation (6G) networks has intensified interest in vehicle-to-everything (V2X) communication, where reconfigurable intelligent surfaces (RIS) are emerging as a key enabling technology. However, dynamic blockages in urban environments pose a critical challenge for vehicle-to-vehicle (V2V) and vehicle-to-infrastructure (V2I) links. Buildings, large vehicles, and roadside obstacles induce frequent line-of-sight (LOS) to non-line-of-sight (NLOS) transitions, causing sharp attenuation and rate fluctuations [2]. These losses have been quantified in measurements: Boban et al. [3] report 5–25 dB vehicle-induced attenuation from 6.75 GHz to 73 GHz; Rodriguez et al. [4] measured 17–25 dB fading at 28 GHz depending on vehicle height; and Liu et al. [5] report 10–20 dB additional loss from truck obstructions at mmWave frequencies.

Intelligent reflecting surfaces (IRS) have emerged as a promising approach to control the propagation environment through passive planar arrays that impose programmable phase shifts on incident waves, enabling reflection steering without RF chains [6]. Under Rician fading, Singh et al. derive closed-form ergodic-capacity expressions for RIS-assisted links and show that the effective channel becomes less random as the number of reflecting elements increases, which is relevant to LOS-dominant vehicular scenarios [7].

The 3GPP TR 38.901 Urban Microcell (UMi) Street Canyon model [8] is widely used as a baseline for mmWave urban links and is discussed in the context of vehicular mmWave path-loss modeling by Giordani et al. [9]. Boban et al. [10] develop a three-state Markov chain for LOS/NLOSv/NLOSb transitions trained on over 10^6 V2V links across multiple cities. Field measurements by Zhu et al. [11] report mean Rician K-factors of 1.8–3 dB across urban, suburban, and rural environments, supporting the use of moderate K-factor values in analytical studies.

Moreover, Tian et al. [12] optimize RIS deployment in mmWave vehicular systems with random vehicle blockages, showing that placement parameters (including height) can enhance coverage and reliability by creating an alternative reflected path. Mensi and Rawat [13] study RIS selection for vehicular communications and derive closed-form expressions for ergodic capacity and symbol error probability

DOI: 10.13164/re.2026.0184

to quantify the benefit of selecting an appropriate surface among multiple candidates. Shaikh et al. [14] analyze dual-RIS-assisted V2I communication under Nakagami-m fading through closed-form performance evaluation. Vishwakarma et al. [15] investigate STAR-RIS-NOMA empowered V2V communications over cascaded double-Rayleigh fading and characterize outage/capacity behavior as a function of the number of reconfigurable elements. Dong et al. [16] develop an analytical vehicular blockage modeling framework for mmWave V2V links that captures the impact of traffic-induced obstructions and antenna placement on link quality.

Despite advances in V2V channel measurement, RIS-aided vehicular link design, and RIS deployment optimization, many existing studies assume either fixed LOS or fixed NLOS conditions and do not capture the dynamic LOS/NLOS transitions characteristic of realistic urban vehicular scenarios. An open question therefore remains: *when and where does IRS provide the greatest benefit?* Specifically, are IRS gains roughly uniform across propagation regimes, or do they concentrate in blockage situations where the direct path is severely attenuated? Quantifying this regime dependence is essential for practical IRS deployment.

In this paper, we develop a modeling-and-simulation framework to quantify regime-dependent IRS gains under dynamic urban blockage. Large-scale path loss follows the 3GPP TR 38.901 UMi Street Canyon model, small-scale fading is Rician with $K = 2$, consistent with urban K-factor measurements in [11], and dynamic blockage is modeled via three spatial NLOS zones in which the direct path incurs an additional 15 dB blockage loss, chosen as a representative value consistent with reported mmWave vehicular blockage-loss measurements (5–25 dB [3], 17–25 dB [4], and 10–20 dB [5]). The vehicle–IRS and IRS–BS links are assumed unblocked under elevated roadside IRS placement. The main contributions of this paper are listed as follows:

- A dynamic blockage model comprising three spatial NLOS zones, with blockage-loss parameters motivated by published mmWave vehicular measurements [3–5], enabling tractable analysis of LOS/NLOS transitions.
- A regime-dependent performance analysis methodology that separately quantifies IRS gains under LOS and NLOS conditions via trajectory-based simulation, revealing improvement ratios differing by approximately an order of magnitude.
- A hypothesis-driven analysis framework that predicts asymmetric IRS effectiveness, reduced CSI sensitivity under blockage, and superlinear scaling with obstruction severity, validated through Monte Carlo simulation.
- Deployment guidelines identifying blockage severity thresholds (e.g., >20 dB) for effective IRS placement; the qualitative principle generalizes, though precise thresholds may vary across environments.

The reported gains and thresholds are conditioned on the adopted 3GPP UMi model and unblocked IRS assumptions; quantitative results may differ under alternative channel models or obstructed IRS links.

The remainder of this paper is organized as follows. In Sec. 2, the system model and the dynamic blockage characterization are presented. In Sec. 3, the proposed analysis framework is developed. The simulation results and deployment guidelines are provided in Sec. 4, and Section 5 concludes this paper.

2. System Model and Channel Characterization

2.1 Network Geometry

We consider an IRS-aided V2I uplink as illustrated in Fig. 1, operating at carrier frequency $f_c = 24.2$ GHz, representative of 5G NR frequency range 2 (FR2) allocations for V2X. The system consists of a single-antenna vehicle, a base station (BS) equipped with $N_r = 2$ receive antennas, and an IRS comprising $M \times N = 16 \times 16$ passive reflecting elements arranged in a uniform planar array (UPA). The inter-element spacing is set to $\Delta = 0.5\lambda$, where $\lambda = c/f_c \approx 12.4$ mm.

Node positions in Cartesian coordinates are specified as

$$\begin{aligned} \mathbf{p}_{\mathrm{BS}} &= [20, -10, 12]^{\mathrm{T}}\ \mathrm{m}, \\ \mathbf{p}_{\mathrm{IRS}} &= [0, 0, 4]^{\mathrm{T}}\ \mathrm{m}, \\ \mathbf{p}_{\mathrm{V}} &= [1.5, y, 1]^{\mathrm{T}}\ \mathrm{m}, \quad y \in [-50, 50]\ \mathrm{m}. \end{aligned} \tag{1}$$

The positions of the network nodes are illustrated in Fig. 2. We adopt a right-handed Cartesian coordinate system in which the y-axis is aligned with the vehicle trajectory (road direction), the x-axis denotes the lateral direction across the road, and the z-axis denotes height. The origin $(0, 0, 0)$ is defined on the ground directly below the IRS reference point. The IRS is mounted on the yz-plane ($x = 0$) with reference

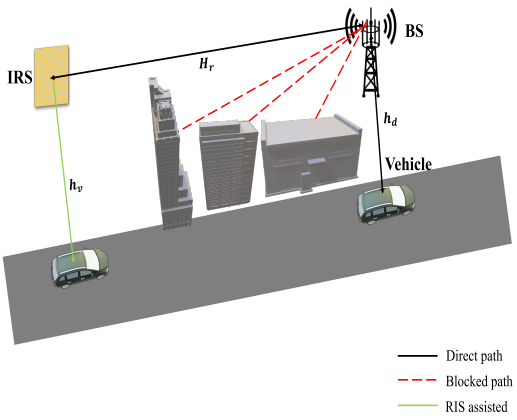

Fig. 1. IRS-assisted V2I communication scenario with building-induced blockage.

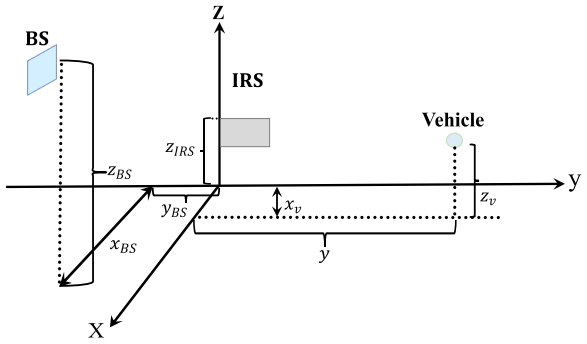

Fig. 2. Network geometry with BS, IRS, and vehicle trajectory.

point $\mathbf{p}_{\mathrm{IRS}} = [0, 0, 4]^{\mathrm{T}}$ m, representing elevated roadside infrastructure (e.g., lamp posts or building-mounted surfaces) positioned above common ground-level obstructions [12]. Elevated IRS deployments are widely considered in vehicular communications surveys [6]. The vehicle travels along the y-axis with fixed lateral offset $x_{\mathrm{V}} = 1.5$ m and antenna height $z_{\mathrm{V}} = 1$ m over $y \in [-50, 50]$ m, representing a single-lane road segment. The BS height of 12 m is typical of urban microcell deployments and falls within ranges considered in IRS-aided vehicular studies (e.g., 8–12 m in [12]). The choice $z_{\mathrm{V}} = 1$ m serves as a simplified baseline between bumper-level and rooftop-level placements commonly considered in urban vehicular evaluations (e.g., 0.75 m and 1.6 m in [2]).

This single-lane, single-IRS geometry is adopted as a controlled baseline to isolate the impact of time-varying blockage on the direct and cascaded (BS–IRS–vehicle) links, while keeping the model tractable and reproducible.

2.2 Channel Model

Let $\mathbf{h}_d \in \mathbb{C}^{N_{\mathrm{r}} \times 1}$ denote the vehicle–BS channel, $\mathbf{h}_v \in \mathbb{C}^{MN \times 1}$ the vehicle–IRS channel, and $\mathbf{H}_r \in \mathbb{C}^{N_{\mathrm{r}} \times MN}$ the IRS–BS channel. Small-scale fading is modeled as Rician with baseline $K = 2$ (linear, ≈ 3 dB), representative of a moderate LOS condition in urban microcell settings (e.g., WINNER II UMi Scenario B1 uses $K \approx 3.3$ dB) [17]. A common baseline K is used for all links in this study; using link-specific K values only affects the LOS/NLOS power split in (2).

$$\mathbf{H} = \sqrt{\frac{K}{K+1}}\mathbf{H}_{\mathrm{LOS}} + \sqrt{\frac{1}{K+1}}\mathbf{H}_{\mathrm{NLOS}} \tag{2}$$

where $\mathbf{H}$ represents any of the three channels with appropriate dimensions.

Path loss follows the 3GPP UMi Street Canyon model (TR 38.901) [8], used as a standardized large-scale baseline for the considered FR2 carrier and microcell geometry. While site-specific vehicular measurements may yield different absolute loss values, the conversion from path loss to channel amplitude in (5) is unchanged.

$$\mathrm{PL}_{\mathrm{LOS}}(\mathrm{dB}) = 32.4 + 21\log_{10}(d) + 20\log_{10}(f_{\mathrm{c}}), \tag{3}$$

$$\mathrm{PL}_{\mathrm{NLOS}}(\mathrm{dB}) = \max\Big\{\mathrm{PL}_{\mathrm{LOS}},\ 22.4 + 35.3\log_{10}(d) + 21.3\log_{10}(f_{\mathrm{c}}) - 0.3(h_{\mathrm{ut}} - 1.5)\Big\} \tag{4}$$

where d is in m, f_{c} is in GHz, and $h_{\mathrm{ut}} = 1$ m is the vehicle antenna height.

The path loss in (3)–(4) specifies the average large-scale power attenuation. Thus, for $s \in \{\mathrm{LOS}, \mathrm{NLOS}\}$, we compute the linear power gain and the complex-baseband amplitude scaling as

$$\begin{aligned} \beta_s(d) &= 10^{-\mathrm{PL}_s(\mathrm{dB})/10}, \\ \alpha_s(d) &= \sqrt{\beta_s(d)} = 10^{-\mathrm{PL}_s(\mathrm{dB})/20} \end{aligned} \tag{5}$$

where $\beta_s(d)$ is the linear power gain and $\alpha_s(d)$ is the corresponding complex-baseband amplitude scaling for $s \in \{\mathrm{LOS}, \mathrm{NLOS}\}$. Moreover, $\mathbf{a}_{\mathrm{rx}}(\theta, \phi)$ and $\mathbf{a}_{\mathrm{tx}}(\theta, \phi)$ denote the unit-norm steering vectors of the receive and transmit arrays (BS ULA and IRS UPA), obtained from the Cartesian geometry in Fig. 2 using standard ULA/UPA array responses.

For the SIMO links $\mathbf{h}_d$ and $\mathbf{h}_v$ (single-antenna transmitter), the LOS component is

$$\mathbf{h}_{\mathrm{LOS}} = \alpha_{\mathrm{LOS}}(d)\ \exp(-\mathrm{j}2\pi d/\lambda)\,\mathbf{a}_{\mathrm{rx}}(\theta, \phi) \tag{6}$$

where $\alpha_{\mathrm{LOS}}(d)$ is obtained from (5). For the MIMO link $\mathbf{H}_r$, we use a rank-one LOS model.

$$\mathbf{H}_{\mathrm{LOS}} = \alpha_{\mathrm{LOS}}(d)\ \exp(-\mathrm{j}2\pi d/\lambda)\,\mathbf{a}_{\mathrm{rx}}(\theta, \phi)\mathbf{a}_{\mathrm{tx}}^{H}(\theta, \phi). \tag{7}$$

The diffuse (NLOS) component is modeled as i.i.d. circularly symmetric complex Gaussian fading (Rayleigh envelope) [18]:

$$\mathbf{H}_{\mathrm{NLOS}} = \alpha_{\mathrm{NLOS}}(d)\,\frac{1}{\sqrt{2}}(\mathbf{X} + \mathrm{j}\mathbf{Y}) \tag{8}$$

where $\mathbf{X}$ and $\mathbf{Y}$ have dimensions matching $\mathbf{H}_{\mathrm{NLOS}}$ and have i.i.d. entries distributed as $\mathcal{N}(0, 1)$, and $\alpha_{\mathrm{NLOS}}(d)$ is obtained from (5).

2.3 Dynamic Blockage Model

To emulate building-induced LOS/NLOS transitions along the vehicle trajectory in a controlled and repeatable manner, we define three spatial NLOS zones on the road axis:

$$y \in [-40, -25]\ \mathrm{m}, \quad y \in [-10, 5]\ \mathrm{m}, \quad y \in [25, 35]\ \mathrm{m}. \tag{9}$$

When the vehicle is within these zones, the direct vehicle–BS link is modeled with an additional shadowing loss of $\Delta_{\mathrm{blk}} = 15$ dB, i.e.,

$$\mathbf{h}_d^{(\mathrm{blk})} = \alpha_b \mathbf{h}_d, \qquad \alpha_b = 10^{-\Delta_{\mathrm{blk}}/20}. \tag{10}$$

Outside blockage zones, $\mathbf{h}_d^{(\mathrm{blk})} = \mathbf{h}_d$. The value $\Delta_{\mathrm{blk}} = 15\,\mathrm{dB}$ is selected as a representative, moderate blockage level, consistent with reported mmWave vehicular blockage/shadowing magnitudes on the order of ∼10–20 dB depending on geometry and obstructing objects [4], [5].

The zone boundaries in (9) are a baseline configuration used to create repeated, spatially localized blockage events for reproducible comparison between the direct and IRS-assisted paths. Changing Δ_{blk} or the zone placement primarily affects quantitative performance (e.g., the frequency and severity of direct-link degradation) but preserves the underlying mechanism under study.

In the baseline model, blockage is applied only to the ground-level BS–vehicle link. The IRS-related sublinks ($\mathbf{h}_v$ and $\mathbf{H}_r$) are modeled as unblocked due to an elevated roadside/building-mounted IRS deployment, which is commonly adopted as a baseline assumption in RIS-assisted vehicular studies to reduce near-ground obstructions [6].

2.4 Signal Model and IRS Phase Design

The vehicle transmits symbol x with $\mathbb{E}\{|x|^2\} = 1$ and power P_{tx}. The IRS applies a diagonal phase-shift matrix $\mathbf{\Phi} = \mathrm{diag}(\mathbf{v})$, where $\mathbf{v} = [v_1, \ldots, v_{MN}]^{\mathrm{T}}$ and $v_n = \exp(\mathrm{j}\phi_n)$ with $|v_n| = 1$. The received signal at the BS is

$$\mathbf{y} = \sqrt{P_{\mathrm{tx}}}\,\mathbf{h}_{\mathrm{eff}} x + \mathbf{n} \tag{11}$$

where $\mathbf{n} \sim \mathcal{CN}(\mathbf{0}, \sigma_{\mathrm{n}}^2\mathbf{I})$ and σ_{n}^2 denotes the noise power per receive antenna. The effective channel is

$$\mathbf{h}_{\mathrm{eff}} = \mathbf{h}_d^{(\mathrm{blk})} + \mathbf{H}_r\ \mathrm{diag}(\mathbf{h}_v)\,\mathbf{v} \tag{12}$$

where $\mathbf{h}_d^{(\mathrm{blk})}$ denotes the direct channel under the blockage state (LOS/NLOS), and $\mathbf{h}_v$ is the IRS–vehicle channel vector. Using maximum ratio combining (MRC), we set $\mathbf{w} = \mathbf{h}_{\mathrm{eff}}/\|\mathbf{h}_{\mathrm{eff}}\|$, which yields the instantaneous SNR

$$\gamma = \frac{P_{\mathrm{tx}}}{\sigma_{\mathrm{n}}^2}\,\|\mathbf{h}_{\mathrm{eff}}\|^2, \tag{13}$$

and the achievable rate

$$R = \log_2(1 + \gamma). \tag{14}$$

The IRS phase vector is optimized to maximize the received power:

$$\begin{aligned} \max_{\mathbf{v}} \quad & \left\|\mathbf{h}_d^{(\mathrm{blk})} + \mathbf{\Psi}\mathbf{v}\right\|^2 \\ \text{s.t.} \quad & v_n \in \{\exp(\mathrm{j}2\pi\ell/L) :\ \ell = 0, \ldots, L-1\} \\ & n = 1, \ldots, MN \end{aligned} \tag{15}$$

where $\mathbf{\Psi} = \mathbf{H}_r\ \mathrm{diag}(\mathbf{h}_v) \in \mathbb{C}^{N_{\mathrm{r}} \times MN}$. We solve (15) using a coordinate-ascent algorithm with $L = 8$ uniformly quantized phase levels (discrete-phase updates) [19].

3. Regime and Sensitivity Analysis

This section analyzes the operating regimes implied by the system model in Sec. 2 and studies the sensitivity of IRS-assisted links to channel knowledge, fading conditions, and blockage severity. We also state hypotheses that are evaluated in Sec. 4.

3.1 Blockage Regimes

From Sec. 2, the MRC-combined SNR is determined by the effective channel $\mathbf{h}_{\mathrm{eff}} = \mathbf{h}_d^{(\mathrm{blk})} + \mathbf{\Psi}\mathbf{v}$, where $\mathbf{h}_d^{(\mathrm{blk})} = \mathbf{h}_d$ outside blockage zones and $\mathbf{h}_d^{(\mathrm{blk})} = \alpha_b\mathbf{h}_d$ inside blockage zones. In unobstructed segments

$$\mathbf{h}_{\mathrm{eff}}^{(\mathrm{LOS})} = \mathbf{h}_d + \mathbf{\Psi}\mathbf{v} \tag{16}$$

and a direct-path-dominant condition corresponds to

$$\|\mathbf{h}_d\| \gg \|\mathbf{\Psi}\mathbf{v}\| \tag{17}$$

in which the IRS mainly provides an auxiliary coherent contribution. In blockage zones

$$\mathbf{h}_{\mathrm{eff}}^{(\mathrm{blk})} = \alpha_b\mathbf{h}_d + \mathbf{\Psi}\mathbf{v} \approx \mathbf{\Psi}\mathbf{v}, \qquad (\alpha_b \ll 1) \tag{18}$$

which represents an IRS-path-dominant regime. The regime-dependent IRS gains are quantified using the rate ratios

$$G_{\mathrm{IRS}}^{(\mathrm{LOS})} = \frac{R_{\mathrm{with\,IRS}}^{(\mathrm{LOS})}}{R_{\mathrm{without\,IRS}}^{(\mathrm{LOS})}}, \tag{19}$$

$$G_{\mathrm{IRS}}^{(\mathrm{blk})} = \frac{R_{\mathrm{with\,IRS}}^{(\mathrm{blk})}}{R_{\mathrm{without\,IRS}}^{(\mathrm{blk})}}. \tag{20}$$

Under the baseline assumption that blockage mainly attenuates the ground-level direct link while the IRS-related sublinks remain LOS-dominant, it is expected that $G_{\mathrm{IRS}}^{(\mathrm{blk})}$ exceeds $G_{\mathrm{IRS}}^{(\mathrm{LOS})}$ when the blockage is sufficiently strong. The gap between $G_{\mathrm{IRS}}^{(\mathrm{blk})}$ and $G_{\mathrm{IRS}}^{(\mathrm{LOS})}$ is shaped by the blockage depth, IRS placement, and any additional attenuation affecting the IRS sublinks; these effects are quantified in Sec. 4 via trajectory, distributional, and gain-based evaluations.

3.2 CSI under Blockage

Acquiring full CSI for IRS-assisted links can be costly due to training and feedback overhead. Motivated by location-assisted IRS control methods [20], we consider a location-based LOS-only baseline, in which the IRS configuration relies only on deterministic LOS components inferred from node locations:

$$\hat{\mathbf{h}}_d = \mathbf{h}_{d,\mathrm{LOS}}, \qquad \hat{\mathbf{H}}_r = \mathbf{H}_{r,\mathrm{LOS}}, \qquad \hat{\mathbf{h}}_v = \mathbf{h}_{v,\mathrm{LOS}}. \tag{21}$$

The IRS phase vector is optimized using these LOS-only estimates, while performance is evaluated on the full fading channels.

To quantify CSI sensitivity, we define the absolute rate degradation

$$\Delta R = R_{\text{full CSI}} - R_{\text{position-based CSI}} \quad (\text{bits/s/Hz}). \tag{22}$$

To connect this behavior to the underlying channel composition, we decompose the effective channel into deterministic and diffuse parts, $\mathbf{h}_{\text{eff}} = \mathbf{h}_{\text{eff,LOS}} + \mathbf{h}_{\text{eff,NLOS}}$, consistent with the standard Rayleigh/Rician fading interpretation [18]. We then define an effective Rician factor for the composite channel as

$$K_{\text{eff}} \triangleq \frac{\mathbb{E}\{\|\mathbf{h}_{\text{eff,LOS}}\|^2\}}{\mathbb{E}\{\|\mathbf{h}_{\text{eff,NLOS}}\|^2\}}. \tag{23}$$

Inside blockage zones, the direct-link contribution is scaled by α_b and its power is reduced approximately by α_b^2, while the reflected term is governed by the IRS sublinks in the baseline model. Consequently, decreasing α_b tends to reduce the relative weight of the attenuated direct diffuse component and increase the determinism of the composite channel, motivating the hypothesis that position-based CSI incurs a smaller penalty under blockage:

$$\Delta R^{(\text{blk})} < \Delta R^{(\text{LOS})}. \tag{24}$$

For compact comparison across blockage levels, we also report the normalized reduction

$$\eta_{\text{reduction}} = \frac{\Delta R^{(\text{LOS})} - \Delta R^{(\text{blk})}}{\Delta R^{(\text{LOS})}} \times 100\%. \tag{25}$$

3.3 *K*-Factor Dependence

The Rician K-factor is defined as the ratio between deterministic (LOS) and diffuse (scattered) power. Under the adopted per-link Rician model (with independent LOS/NLOS components), the average received power of the direct channel satisfies

$$\begin{aligned}\mathbb{E}\left[\|\mathbf{h}_d\|^2\right] &= \frac{K}{K+1}\|\mathbf{h}_{d,\text{LOS}}\|^2 \\ &\quad + \frac{1}{K+1}\mathbb{E}\left[\|\mathbf{h}_{d,\text{NLOS}}\|^2\right].\end{aligned} \tag{26}$$

Showing that smaller K increases the relative contribution of diffuse scattering. In blockage zones, the direct link is downweighted by α_b and thus contributes less to $\mathbf{h}_{\text{eff}}$, so the performance of the IRS-assisted link is expected to be less sensitive to scattering than the direct-only baseline. At the same time, because the reflected term is itself subject to small-scale fading on both sublinks, a moderate K-dependence of the IRS gain can persist. These trends are evaluated in Sec. 4 by sweeping K over a practical range and comparing trajectory-averaged performance under unobstructed and blockage conditions.

3.4 Blockage Severity Scaling

We define $\alpha_b = 10^{-\Delta_{\text{dB}}/20}$ as the direct-link amplitude attenuation in blockage zones, where Δ_{dB} denotes the blockage depth (dB). The direct-only baseline rate under blockage is approximated as

$$R_{\text{no IRS}}^{(\text{blk})} \approx \log_2\left(1 + \frac{P_{\text{tx}}}{\sigma_{\text{n}}^2}\alpha_b^2\|\mathbf{h}_d\|^2\right) \tag{27}$$

while the IRS-assisted rate can be approximated as

$$R_{\text{IRS}}^{(\text{blk})} \approx \log_2\left(1 + \frac{P_{\text{tx}}}{\sigma_{\text{n}}^2}\|\mathbf{H}_r\mathbf{\Phi}\mathbf{h}_v\|^2\right) \tag{28}$$

which is only weakly dependent on α_b in the baseline model where blockage primarily affects the direct link. We define the blockage-dependent IRS gain as

$$G_{\text{IRS}}(\Delta_{\text{dB}}) = \frac{R_{\text{IRS}}^{(\text{blk})}}{R_{\text{no IRS}}^{(\text{blk})}}. \tag{29}$$

Since $\log_2(1+x)$ is increasing, $R_{\text{no IRS}}^{(\text{blk})}$ in (27) decreases as the blockage depth Δ_{dB} increases (equivalently, as α_b decreases). In contrast, $R_{\text{IRS}}^{(\text{blk})}$ in (28) is approximately insensitive to Δ_{dB} in the baseline model where blockage primarily affects the direct link. Consequently, $G_{\text{IRS}}(\Delta_{\text{dB}})$ in (29) is expected to increase with blockage severity over the considered range, which motivates the empirical fit in (30).

Motivated by the contrasting α_b-dependence in (27)–(28), we use a power-law form as an empirical fit over the simulated blockage range:

$$G_{\text{IRS}}(\Delta_{\text{dB}}) \propto \alpha_b^{-\beta} \tag{30}$$

where the exponent β is obtained by regression on simulation results and is used as a trend descriptor rather than a universal constant.

Finally, the IRS array size influences the reflected term through coherent combining across reflecting elements. Under phase alignment, the reflected-path power is commonly approximated to scale with the squared aperture (up to geometry- and path-loss-dependent factors), motivating

$$\|\mathbf{H}_r\mathbf{\Phi}\mathbf{h}_v\|^2 \propto (MN)^2. \tag{31}$$

Accordingly, larger IRS arrays are expected to yield stronger gains under severe blockage and a steeper gain-versus-blockage trend. Section 4 evaluates this behavior using two representative IRS sizes (8×8 and 16×16) and a sweep over blockage severities.

4. Numerical Results

4.1 Simulation Setup

We evaluate the proposed model and simulation framework via Monte Carlo simulations. Each data point is obtained by averaging 50 independent channel realizations per vehicle position. The system operates at carrier frequency $f_c = 24.2$ GHz (5G NR FR2), with transmit power $P_{\text{tx}} = 30$ dBm and noise power per receive antenna $\sigma_{\text{n}}^2 = -104$ dBm over $B = 10$ MHz. The noise power is computed from the thermal noise density $N_0 = -174$ dBm/Hz as

$N_0 + 10\log_{10}(B) \approx -104$ dBm. Two IRS configurations are considered: 16×16 (256 elements) and 8×8 (64 elements), both with half-wavelength spacing $\Delta = 0.5\lambda$. The BS employs $N_r = 2$ antennas with MRC. All simulations and figure generation were carried out in MATLAB, implementing the adopted channel model and phase-optimization algorithm.

The vehicle moves along $y \in [-50, 50]$ m with 0.5 m spatial resolution, yielding 200 evaluation positions. Three blockage zones, located at $y \in [-40, -25]$ m, $y \in [-10, 5]$ m, and $y \in [25, 35]$ m, impose 15 dB attenuation on the direct V2I path. All links experience Rician small-scale fading with $K = 2$. Large-scale path loss follows the 3GPP TR 38.901 UMi Street Canyon model [8]. IRS phase optimization is performed with finite-resolution (3-bit) discrete phase shifts ($L = 8$) using an iterative coordinate-wise update procedure [19], with a maximum of 100 iterations.

4.2 IRS Gains in LOS/NLOS

Figure 3 shows the achievable rate along the vehicle route with three blockage-induced LOS/NLOS transitions (shaded regions). In the blocked zones, the direct-only link (red dashed) drops sharply and approaches near outage, whereas the IRS-assisted link (blue solid) remains substantially higher, confirming the regime-dependent behavior predicted in Sec. 3.1. The corresponding 95% confidence intervals are tight (within ±0.002 bits/s/Hz), indicating stable Monte Carlo estimates.

Figure 4 presents the CDFs under LOS and blockage-defined NLOS conditions, and Figure 5 quantifies the corresponding IRS gains. In LOS, the IRS provides a modest 1.18× improvement (mean rate from 0.96 to 1.13 bits/s/Hz), whereas under blockage the gain increases to 10.79× (mean rate from 0.08 to 0.91 bits/s/Hz). The resulting differential gain ratio is

$$\frac{G_{\text{IRS}}^{(\text{NLOS})}}{G_{\text{IRS}}^{(\text{LOS})}} \approx 9.1. \tag{32}$$

This pronounced asymmetry arises because the direct path already provides a strong signal level in unobstructed segments, limiting the marginal contribution of the IRS-reflected component. Under blockage, the direct-link power drops by $\alpha_b^2 \approx -30$ dB, so the baseline rate collapses to near outage and the IRS-reflected path becomes the dominant term in $\|\mathbf{h}_{\text{eff}}\|^2$. The IRS thus effectively substitutes for the lost direct path rather than merely supplementing it, which explains the order-of-magnitude difference in relative gain between regimes.

This behavior is consistent with the general finding in the RIS vehicular literature that passive surfaces yield the largest relative gains when the alternative path is weakest [6]. An approximately 50% area-averaged rate improvement under optimized RIS deployment at 60 GHz with random truck blockages is reported in [12]; however, their single trajectory-averaged metric does not distinguish between LOS and NLOS contributions. Our regime-separated analysis reveals that averaged metrics mask the underlying differential: the IRS benefit concentrates almost entirely in blockage zones, where it restores the mean rate from near outage to a level comparable with unobstructed operation, as illustrated in Fig. 6.

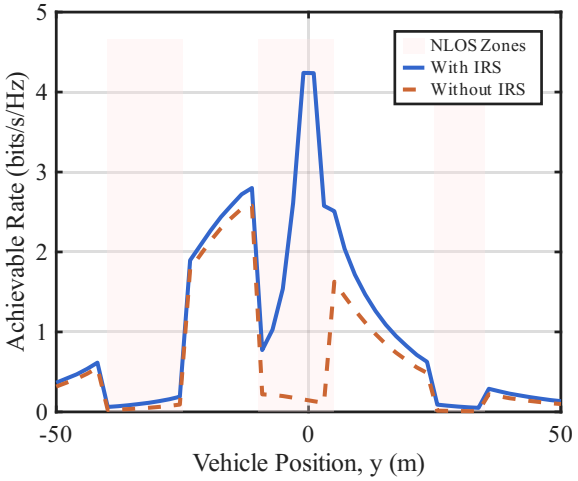

Fig. 3. Achievable rate along vehicle trajectory. Shaded regions indicate blockage zones.

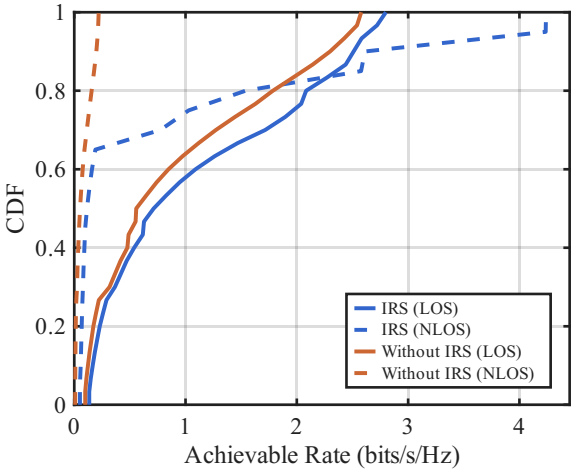

Fig. 4. CDF of achievable rate under LOS and NLOS conditions.

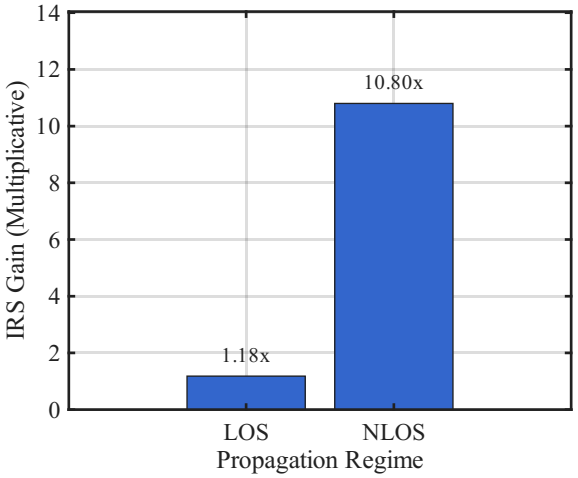

Fig. 5. IRS gain under LOS and NLOS conditions.

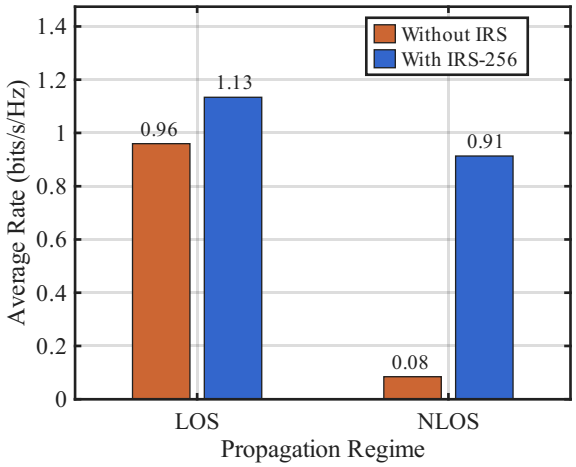

Fig. 6. Mean achievable rate under LOS and NLOS conditions.

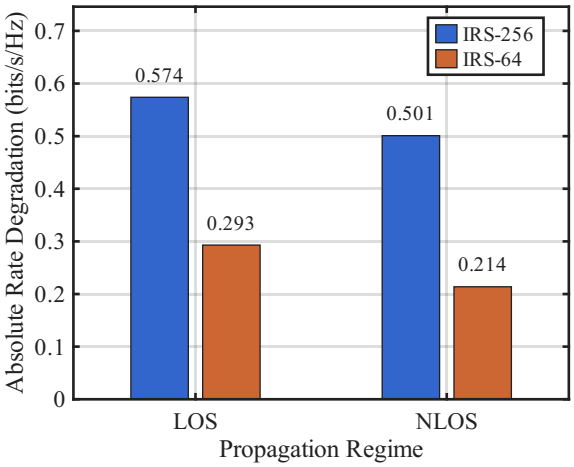

Fig. 7. CSI degradation under LOS and NLOS for IRS-256 and IRS-64.

Similarly, Mensi and Rawat [13] report ergodic capacity of 0.45–2.25 bits/s/Hz for RIS-aided vehicular links depending on array size (50–500 elements) under correlated Rayleigh fading, which brackets the absolute rates observed here and corroborates that the IRS-assisted performance scale is representative of comparable settings.

4.3 CSI Impact

Position-based CSI is evaluated according to (21). The IRS phase shifts are optimized using these coarse estimates, whereas the achievable rate is computed using the full fading realization. Figure 7 shows the absolute rate loss ΔR in both LOS and NLOS for the two IRS sizes. For IRS-256, position-based CSI yields a loss of 0.574 bits/s/Hz in LOS, which decreases to 0.501 bits/s/Hz in NLOS (12.7% reduction). For IRS-64, the loss decreases from 0.293 to 0.214 bits/s/Hz (27.0% reduction). Figure 8 confirms this trend distributionally: in LOS, full CSI provides a distinct rightward shift over position-based CSI, whereas in blockage zones the two CDFs become much closer and partially overlap.

The reduced CSI penalty under blockage is explained by the change in channel composition. When the direct path is attenuated by α_b, its diffuse component contributes less power to $\mathbf{h}_{\text{eff}}$, and the IRS-reflected path—which retains its LOS-dominant structure—becomes the primary term. This effectively increases the determinism of the composite channel (cf. K_{eff} in (23)), making position-based phase optimization a closer approximation to the full-CSI solution. The stronger robustness of IRS-64 (27.0%) compared with IRS-256 (12.7%) further reflects the lower optimization dimensionality of smaller arrays, which makes the phase solution less sensitive to CSI imperfections.

This observation aligns with the position-aided IRS control framework studied by Xing et al. [20], who show that location information can substitute for instantaneous CSI with limited performance loss when the channel has a strong deterministic component. In vehicular settings, where coherence time is short due to mobility and beam-training overhead scales with the number of IRS elements, the ability to maintain near-optimal performance with coarser channel knowledge in blockage zones—precisely where IRS assistance is most needed—represents a favorable trade-off between overhead and gain.

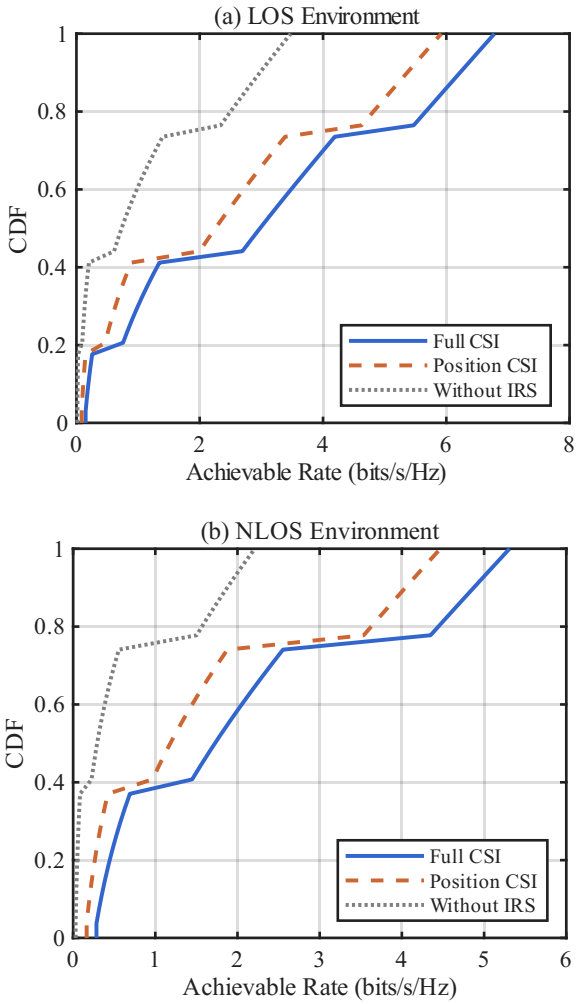

Fig. 8. CDF of achievable rate under full CSI and position-based CSI.

4.4 K-Factor Impact

The influence of the scattering environment is evaluated by sweeping the Rician K-factor over $K \in \{0.5, 1, 2, 5, 10\}$. As shown in Fig. 9 and Tab. 1, the IRS gain in LOS is largely insensitive to K, remaining around 1.37–1.40× over the tested range. In contrast, the NLOS gain increases monotonically with K, from 1.29× at $K = 0.5$ to 1.75× at $K = 10$. Across all K, the IRS-aided NLOS rate remains around 1.5–2.0 bits/s/Hz, while the corresponding baseline without IRS remains around 1.1–1.2 bits/s/Hz.

The near-invariance of the LOS gain indicates that in unobstructed conditions, the IRS contribution is governed primarily by large-scale geometry (path loss and array aperture) rather than small-scale fading statistics. In NLOS, the monotonic increase with K reflects improved coherent combining efficiency: a stronger specular component on the IRS sublinks allows the phase-aligned reflected path to capture a larger share of the available channel power, consistent with the analytical observation of Singh et al. [7] that the effective channel of an RIS-assisted link becomes increasingly deterministic as K grows.

From a deployment perspective, the stability of the IRS-aided NLOS rate across the tested K range (1.5–2.0 bits/s/Hz) is significant because it indicates that the IRS benefit does not critically depend on the precise scattering environment. Urban microcell measurements by Zhu et al. [11] report K-factor values of 1.8–3 dB across urban, suburban, and rural environments, which falls within the range where the IRS consistently provides meaningful NLOS improvement. Even under rich scattering ($K = 0.5$), the IRS-assisted NLOS rate remains above the unblocked direct-link baseline, confirming that passive reflecting surfaces retain practical utility across propagation conditions representative of real vehicular scenarios.

4.5 Scaling Impact

Blockage severity is varied from 10 to 25 dB. In this experiment, only the direct BS–vehicle link is affected by blockage, while the BS–IRS and IRS–vehicle links are assumed unobstructed. The direct link attenuation is modeled as $\alpha_b = 10^{-\Delta/20}$, where Δ is the blockage loss in dB.

Figure 10 and Table 2 show that the IRS gain increases as blockage becomes stronger. Specifically, the IRS-256 gain rises from 1.18× at 10 dB to 3.89× at 25 dB, whereas IRS-64 increases from 1.05× to 1.62×. A power-law fit gives $G(\Delta) \approx c\,\alpha_b^{-\beta}$ with fitted exponents $\beta = 0.69$ (IRS-256) and $\beta = 0.25$ (IRS-64), indicating that larger arrays benefit more when the direct link is more severely attenuated.

The superlinear scaling confirms the analytical prediction in (27)–(31): the IRS-assisted rate in (28) is approximately independent of blockage depth (since only the direct link is attenuated), whereas the baseline rate in (27) collapses as $\alpha_b \to 0$. The fourfold difference in fitted exponents between IRS-256 and IRS-64 ($\beta = 0.69$ vs. 0.25) reflects the squared-aperture scaling $\|\mathbf{H}_r \mathbf{\Phi} \mathbf{h}_v\|^2 \propto (MN)^2$ in (31): larger arrays produce a higher reflected-path power floor, so the gain ratio grows more steeply as the direct-link baseline degrades. With finite-resolution phase shifts (3-bit, $L = 8$) and realistic path-loss geometry, these results confirm that substantial scaling benefits persist under practical constraints.

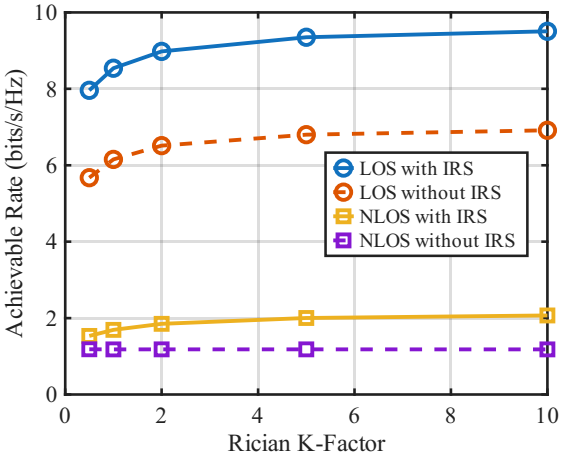

Fig. 9. Achievable rate versus Rician K-factor.

K	LOS Gain (×)	NLOS Gain (×)	Ratio (×)
0.5	1.40	1.29	0.92
1.0	1.39	1.43	1.03
2.0	1.38	1.57	1.14
5.0	1.37	1.69	1.23
10.0	1.37	1.75	1.27

Tab. 1. IRS gain versus Rician K-factor in LOS and blockage-defined NLOS.

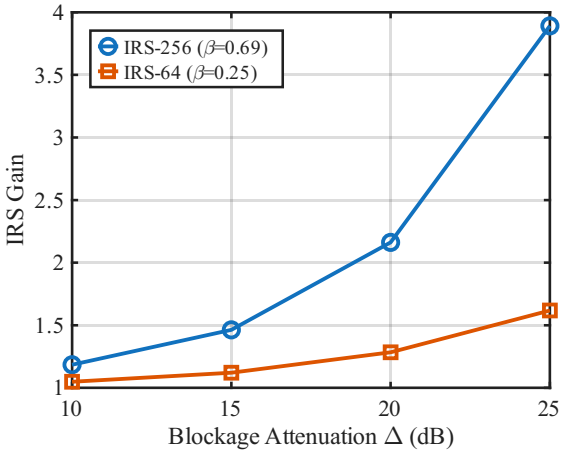

Fig. 10. IRS gain versus blockage attenuation for IRS-256 and IRS-64.

Blk (dB)	G_{256} (×)	G_{64} (×)	R_{256}	R_{64}	R_{dir}
10	1.18	1.05	3.12	2.76	2.63
15	1.46	1.12	2.05	1.57	1.40
20	2.16	1.28	1.31	0.78	0.60
25	3.89	1.62	0.85	0.36	0.22

Tab. 2. Achievable rates and IRS gains versus blockage depth Δ_{dB}.

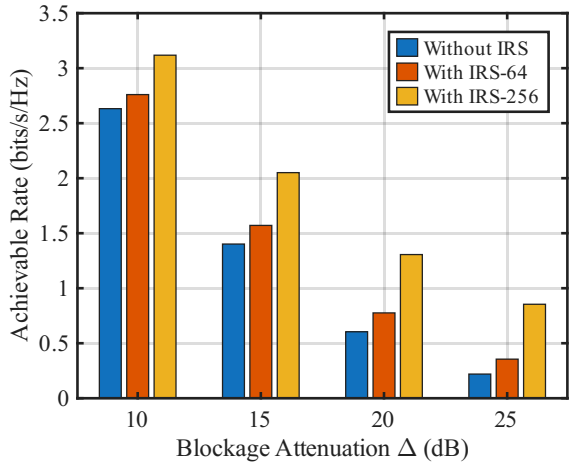

Fig. 11. Achievable rate versus blockage attenuation for baseline and IRS-assisted links.

Figure 11 shows the corresponding absolute rates. At $\Delta = 25$ dB, the baseline drops to 0.22 bits/s/Hz, while IRS-256 sustains 0.85 bits/s/Hz, mitigating the severe rate reduction under deep blockage.

These results provide a quantitative basis for the deployment guideline that IRS panels should be preferentially allocated to locations with consistently high blockage severity, such as urban canyon intersections or tunnel approaches. The observation that IRS-256 exceeds a twofold gain at approximately 20 dB blockage establishes a practical threshold: at sites where measured or predicted blockage exceeds this level, the investment in a 256-element panel yields disproportionate returns compared with smaller arrays. This complements the spatial deployment optimization of Tian et al. [12], who optimize RIS height and downtilt for coverage maximization; our analysis adds blockage severity as an orthogonal deployment dimension that should inform both the placement decision and the choice of array size.

5. Conclusion

This paper evaluated an IRS-aided V2I uplink under trajectory-dependent LOS/NLOS transitions using a tractable system model and Monte Carlo simulations. The results show a clear regime dependence: the IRS provides modest gains in unobstructed segments, but offers substantially larger relative and absolute improvements when the direct path is attenuated by blockage, thereby stabilizing the achievable rate along trajectories with repeated transitions. For the considered setting, the mean NLOS rate improves from 0.08 to 0.91 bits/s/Hz with IRS-256, whereas the LOS increase is from 0.96 to 1.13 bits/s/Hz, yielding $G_{\mathrm{IRS}}^{(\mathrm{NLOS})}/G_{\mathrm{IRS}}^{(\mathrm{LOS})} \approx 9.1$. The corresponding 95% confidence intervals are tight, indicating stable Monte Carlo estimates. Blockage also reduces the marginal benefit of fine-grained CSI, as the performance gap between full CSI and position-based CSI narrows in NLOS, particularly for smaller arrays. Additional parameter sweeps show increasing IRS gains with blockage severity and consistent trends over the tested Rician K-factor range.

These findings should be interpreted within the adopted assumptions, including the 3GPP TR 38.901 UMi Street Canyon path-loss baseline, Rician small-scale fading, and a simplified blockage representation applied to the direct link with a baseline IRS placement and LOS-dominant IRS sublinks. Consequently, the reported numerical gains and fitted scaling exponents are scenario-dependent and require revalidation for different geometries, carrier frequencies, bandwidths, blockage dynamics, and IRS deployments. Future work will therefore focus on (i) sensitivity studies over IRS position/height/orientation and alternative blockage patterns (including gradual and stochastic attenuation and blockage on IRS sublinks), (ii) validation under independent channel models and measurement- or ray-tracing-based environments to translate the observed trends into site-specific deployment rules, and (iii) developing analytical performance bounds (e.g., rate or outage bounds) under dynamic blockage and practical IRS constraints.

Acknowledgments

This work was supported by the National Natural Science Foundation of China under Grant 52102399.

Data Availability Statement: The MATLAB source code used to generate the simulation results in this paper is available from the corresponding author, upon reasonable request.

References

[1] ZHANG, X., CHEN, W., WANG, Y., et al. V2X communication in intelligent connected vehicles: A survey and taxonomy. *Automotive Innovation*, 2025, vol. 8, no. 1, p. 1–25. DOI: 10.1007/s42154-024-00310-2

[2] GARCÍA, M. H. C., MOLINA-GALAN, A., BOBAN, M., et al. A tutorial on 5G NR V2X communications. *IEEE Communications Surveys and Tutorials*, 2021, vol. 23, no. 3, p. 1972–2026. DOI: 10.1109/COMST.2021.3057017

[3] BOBAN, M., DUPLEICH, D., IQBAL, N., et al. Multi-band vehicle-to-vehicle channel characterization in the presence of vehicle blockage. *IEEE Access*, 2019, vol. 7, p. 9724–9735. DOI: 10.1109/ACCESS.2019.2892238

[4] RODRIGUEZ, I., ABASCAL, J. P., CELAYA-ECHARRI, M., et al. Fading statistics of 28 GHz LOS link blockage due to vehicular traffic. *IEEE Transactions on Vehicular Technology*, 2024, vol. 73, no. 11, p. 16120–16130. DOI: 10.1109/TVT.2024.3443612

[5] LIU, Y., SARRIS, C. D., MOLISCH, A. F. Measurements and modeling of mmWave vehicle-to-vehicle channels with vehicle obstructions at 28 GHz. *IEEE Transactions on Wireless Communications*, 2025, vol. 24, no. 2, p. 1050–1065. DOI: 10.1109/TWC.2025.3540968

[6] DENG, Y., NIYATO, D., HAN, Z., et al. RIS-enabled vehicular communications: A comprehensive survey. *IEEE Transactions on Intelligent Vehicles*, 2025, vol. 10, no. 1, p. 1–28. DOI: 10.1109/TIV.2024.3476934

[7] SINGH, A., JAMSHED, M. A., ALI, H., et al. RIS-aided communication: Capacity and performance over Rician fading channels. *arXiv preprint*, 2021, p. 1–8. DOI: 10.48550/arXiv.2107.10937

[8] 3GPP. *Study on channel model for frequencies from 0.5 to 100 GHz*. Technical Report TR 38.901, v15.0.0, June 2018. [Online]. Available at: https://www.3gpp.org/ftp/Specs/archive/38_series/38.901/

[9] GIORDANI, M., SHIMIZU, T., ZANELLA, A., et al. Path loss models for V2V mmWave communication: Performance evaluation and open challenges. In *Proceedings of the IEEE 2nd Connected and Automated Vehicles Symposium (CAVS)*. Honolulu (USA), 2019, p. 1–5. DOI: 10.1109/CAVS.2019.8887792

[10] BOBAN, M., GONG, X., XU, W. Modeling the evolution of line-of-sight blockage for V2V channels. In *Proceedings of the IEEE 84th Vehicular Technology Conference (VTC-Fall)*. Montreal (Canada), 2016, p. 1–7. DOI: 10.1109/VTCFall.2016.7881090

[11] ZHU, S., GHAZAANY, T. S., JONES, S. M. R., et al. Probability distribution of Rician K-factor in urban, suburban and rural areas using real-world captured data. *IEEE Transactions on Antennas and Propagation*, 2014, vol. 62, no. 7, p. 3835–3839. DOI: 10.1109/TAP.2014.2318072

[12] TIAN, X., GONZÁLEZ-PRELCIC, N., HEATH, R. W., Jr., et al. Optimizing the deployment of reconfigurable intelligent surfaces in mmWave vehicular systems. In *Proceedings of the IEEE Global Communications Conference (GLOBECOM)*. Rio de Janeiro (Brazil), 2022, p. 5261–5266. DOI: 10.1109/GLOBECOM48099.2022.10001015

[13] MENSI, N., RAWAT, D. B. Reconfigurable intelligent surface selection for wireless vehicular communications. *IEEE Wireless Communications Letters*, 2022, vol. 11, no. 8, p. 1743–1747. DOI: 10.1109/LWC.2022.3180479

[14] SHAIKH, F. S., RABIE, K., ANSARI, S., et al. On the performance of dual RIS-assisted V2I communication under Nakagami-*m* fading. In *Proceedings of the IEEE 97th Vehicular Technology Conference (VTC-Spring)*. Florence (Italy), 2023, p. 1–6. DOI: 10.1109/VTC2023-Spring57618.2023.10199980

[15] VISHWAKARMA, S. K., YADAV, P., UPADHYAY, P. K. STAR-RIS-NOMA empowered V2V communications over cascaded double Rayleigh fading. *Physical Communication*, 2024, vol. 65, p. 1–11. DOI: 10.1016/j.phycom.2024.102391

[16] DONG, R., SHE, C., HARDJAWANA, W., et al. Vehicular blockage modelling for millimeter wave V2V communications. In *Proceedings of the IEEE International Conference on Communications (ICC)*. Montreal (Canada), 2021, p. 1–6. DOI: 10.1109/ICC42927.2021.9500518

[17] KYÖSTI, P., MEINILÄ, J., HENTILÄ, L., et al. *WINNER II Channel Models*. WINNER II Deliverable D1.1.2, ver. 1.2, Sep. 2007.

[18] SKLAR, B. Rayleigh fading channels in mobile digital communication systems. I. Characterization. *IEEE Communications Magazine*, 1997, vol. 35, no. 7, p. 90–100. DOI: 10.1109/35.620535

[19] DAMPAHALAGE, D., MANOSHA, K. S., RAJATHEVA, N., et al. Intelligent reflecting surface aided vehicular communications. In *Proceedings of the IEEE Global Communications Conference Workshops (GLOBECOM Workshops)*. Taipei (Taiwan), 2020, p. 1–6. DOI: 10.1109/GCWkshps50303.2020.9367569

[20] XING, Z., WANG, R., YUAN, X., et al. Location information assisted beamforming design for reconfigurable intelligent surface aided communication systems. *IEEE Transactions on Wireless Communications*, 2023, vol. 22, no. 11, p. 7676–7695. DOI: 10.1109/TWC.2023.3254526

About the Authors . . .

Diana Kujang SEMAYA received the B.S. degree in Telecommunication Engineering from Huazhong University of Science and Technology (HUST) in 2017, the M.S. degree in Information and Communication Engineering from HUST in 2020, and the M.S. degree in Electronic and Communication Engineering from Wuhan Textile University in 2023. She is currently pursuing the Ph.D. degree at Wuhan University of Technology (WUT). Her research interests include radio channel characterization and modeling, massive MIMO techniques, and intelligent traffic control systems.

Wei CHEN is a Full Professor and Doctoral Supervisor at Wuhan University of Technology (WHUT). He received the Ph.D. degree from Huazhong University of Science and Technology (HUST) in 2005. He holds senior memberships in IEEE and the China Electronics Society, and serves on the Communication and Navigation Standardization Technical Committee under China's Ministry of Transport. His research interests include satellite navigation systems, wireless communications, and intelligent traffic control systems.

Changzhen LI (corresponding author) received the Ph.D. degree in Engineering from Wuhan University of Technology (WUT) in 2020, where he is currently an Associate Professor. In 2019, he was a Visiting Scholar with the Norwegian University of Science and Technology, Trondheim, Norway. His research interests include radio wave propagation, wireless communication, and channel measurement and modeling.